MECHANICAL MODELLING OF RAPID COOLING IN PORCELAIN TILE-TYPE SYSTEMS

Marcelo Dal Bó[1], Vicente Cantavella[2], Enrique Sánchez[2], Dachamir Hotza[1], Anselmo Boschi[3]

[1] Universidade Federal de Santa Catarina (UFSC). Brazil

[2] Instituto de Tecnología Cerámica (ITC). Asociación de Investigación de las Industrias Cerámicas (AICE). Spain

[3] Universidade Federal de São Carlos (UFSCar). Brazil

ABSTRACT

This paper analyses the effect of cooling on mechanical behaviour, in particular, on the residual stresses that appear when materials of the porcelain tile type are involved. However, these compositions have a very complex microstructure, in which there are several crystalline phases and the glassy phase is not homogeneous. In this study a simpler composition was therefore formulated, using sodium feldspar as starting material to which quartz with different particle sizes was added.

A viscoelastic model was used to estimate the residual stresses that develop during cooling. The parameters of the model were obtained either from the literature or were determined in laboratory tests.

An assembly was designed that allowed non-contact measurement of the temperature at the top and bottom surfaces of the test pieces during cooling. The test pieces were subjected to different types of cooling and their residual stresses were then determined by the strain relaxation slotting method.

1. INTRODUCTION

In ceramic tile manufacture, rapid tile cooling is known to lead to residual stresses in the tiles exiting the kiln. This even occurs in products (such as earthenware tile) that give rise to little glassy phase at high temperature. Residual stresses are important because they influence:

- Tile mechanical strength.
- Delayed curvatures, though these depend to a large extent on material creep.
- The cutting process during tile installation. Residual stresses can cause tile cuts to follow undesirable routes or lead to tile breakage.
- Curvature. The removal of stressed areas in rectification or edge-grinding can lead to a change in curvature.

In addition, the arising stresses during tile cooling in the kiln can lead to microstructural damage or even tile breakage.

There are several types of residual stresses, though this study only focuses on one type: the residual stress associated with thermal gradients in the tile during cooling.

2. THEORETICAL MODEL

The theoretical model[1] consists of two phases (Figure 1). In the first, the thermal problem, which consists of calculating the temperature profile, is solved. This requires knowing the geometry of the piece, the thermal properties (thermal conductivity and specific heat), density, and surface temperature as a function of time.

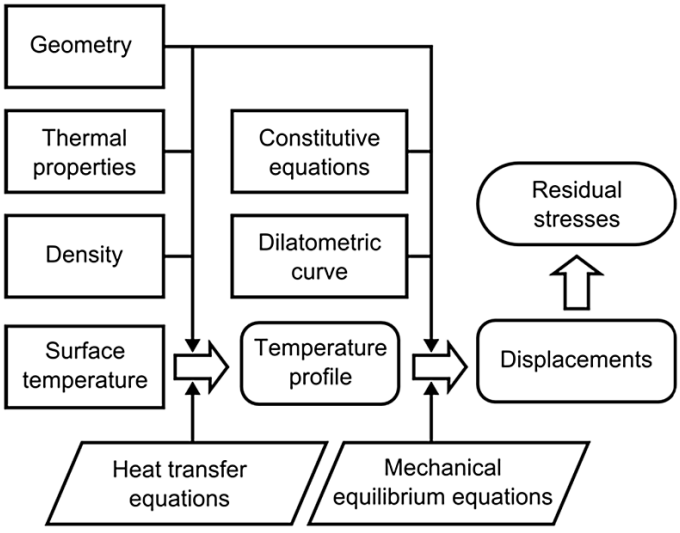

Figure 1. Phases in the calculation of residual stresses.

The equation of non-steady-state heat transfer adopts the form[2]:

$$\frac{\partial T}{\partial t} = \alpha \nabla^2 T$$

Equation 1

where:

T: temperature at a point of the piece at a given time (K)

∇^2 : Laplacian operator (m^{-2})

t: time (s)

α: thermal diffusivity (m^2/s)

Thermal diffusivity α is the quotient between thermal conductivity k (W/(m·K)) and the product of density ρ (kg/m^3) and specific heat c_p (J/(kg·K)): $\alpha = k/(\rho c_p)$.

The second part addresses the mechanical problem, and it determines the shifts of each point of the piece from the mechanical properties (constitutive equations), the dilatometric curve, equilibrium equations, and thermal profile.

The mechanical equilibrium equations derive from the balance of forces and moments applied to the piece[3], and they do not depend on the type of material or its properties. The constitutive equations establish the relationship between the stress and the strain that a body undergoes, and they are a function of the type of material. The simplest law is Hooke's equation (linear elasticity); however, this law is unable to explain how residual stresses are generated. A non-elastic component is required, such as linear viscoelasticity, which leads to the expression:

$$\varepsilon_{e,x} = \frac{1}{E}\sigma_x$$
$$\frac{d\varepsilon_{v,x}}{dt} = \frac{1}{3\eta}\sigma_x$$

Equation 2

where:

$\varepsilon_{e,x}$: elastic strain along the x axis

$\varepsilon_{v,x}$: viscous strain along the x axis

σ_x: normal stress on a perpendicular plane to the x axis (Pa)

E: modulus of elasticity (Pa)

η: viscosity (Pa·s)

There are several equations that relate viscosity to temperature, one of the simplest being[4]:

$$\eta = \eta_0 e^{\Theta / T}$$

Equation 3

where η_0 is the pre-exponential factor (Pa·s) and Θ a constant (K).

The solution of the thermal and mechanical problems requires the use of numerical methods. For the former, finite differences were used and for the latter, the finite element method.

3. EXPERIMENTAL

3.1. Preparation of the test pieces

The test pieces were prepared using sodium feldspar (*Mario Pilato*) as starting material. This was milled with water to an average particle size of 6.4 μm. The material was dried under infrared lamps and then deagglomerated by dry milling for 5 minutes, which did not alter the average particle size. The powder was moistened to 8.0% and pressed at 35 MPa.

The milled feldspar was used to prepare another batch of material to which 20 wt% quartz of different particle sizes (*Sibelco SE-100* and *SE-8*, with average diameters of 13.4 μm and 31 μm, respectively) was added. The materials used in preparing the test pieces are listed in Table 1. The forming process of the test pieces that contained quartz was the same as that of the sodium feldspar test pieces.

Finally, the test pieces were placed in an oven at 110 ºC for at least 2 h, with a view to removing the moisture. They were then fired to the maximum densification temperature (column T_{md} of Table 1).

Composition	Material	T_{md} (ºC)
FdtoNa	Sodium feldspar	1200
FdtoNa-QF	Sodium feldspar +20% Sibelco SE-100 quartz	1205
FdtoNa-QG	Sodium feldspar +20% Sibelco SE-8 quartz	1205

Table 1. Compositions used in preparing the test pieces.

The test pieces were subjected to different types of cooling, inside and outside the kiln. Figure 2 shows the assembly used in cooling outside the kiln. The assembly consisted of a tube with compressed air for cooling the test pieces from the bottom, and two pyrometers (*Raytek model MI320LTS*) that simultaneously measured the top and bottom surface temperature.

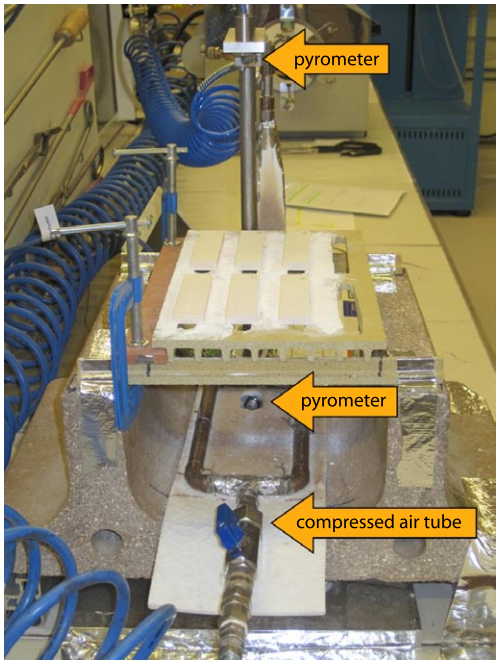

Figure 2. Assembly for temperature measurement during cooling

The following types of cooling were performed:

- **ELL**: Slow cooling, inside the kiln.
- **ELR**: Slow cooling to 650 ºC and rapid cooling (withdrawal of the test pieces from the kiln and cooling with compressed air) from 650 ºC to room temperature.
- **ERR**: Rapid cooling from peak temperature to room temperature.

These types of cooling were designed to separate two phenomena that occur at high cooling rates: the generation of residual stresses and microstructural damage. The former leads to increased mechanical strength, whereas the latter leads to reduced mechanical strength[5].

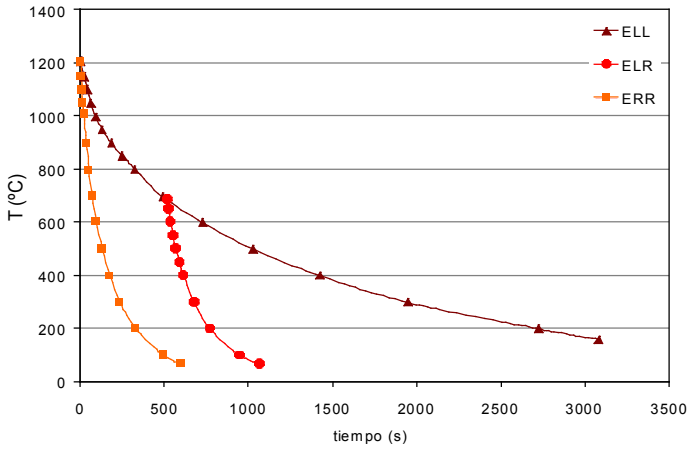

Figure 3. Surface temperature of the test pieces during the different types of cooling

The evolution of the average surface temperature of the test pieces during the different types of cooling is shown in Figure 3.

3.2. Residual stress measurement

The residual stresses were measured by the strain relaxation slotting method (SRSM)[6]. This method has been used elsewhere to measure residual stresses in porcelain tile[5,7]. It consists of adhering a strain gauge to the bottom of the test piece and then cutting slots to an increasing depth (a_i) from the top surface, measuring the strain recorded by the gauge (ε_g) (Figure 4).

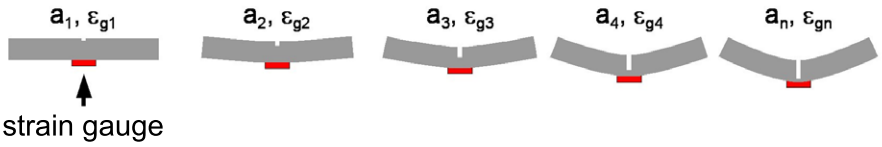

Figure 4. Schematic illustration of the method used to measure the residual stresses.

The residual stresses at a point in the piece (σ_{res}) depend on the position of the point with respect to the centre. That position can be quantified by means of the coordinate ζ, where ζ=0 the centre, ζ=-1 the bottom surface, and ζ=+1 the top surface. σ_{res} can be expressed as a linear combination of Legendre polynomials (P_k) of the coordinate ζ (eq. 4). In ceramic tiles of the porcelain tile type, with conventional cooling it usually suffices to consider only the term of the second degree.

$$\sigma_{res} = -E\sum_{k=2}^{\infty}\lambda_k P_k(\zeta) \cong -E\lambda_2 P_2(\zeta) = \sigma_{sfc} P_2(\zeta) = \sigma_{sfc}\frac{3\zeta^2-1}{2}$$

Equation 4

The residual stress at the surface is σ_{sfc}=-Eλ_2 and, therefore, the complete residual stress profile can only be expressed as a function of the surface stress.

4. DETERMINATION OF MODEL PARAMETERS

4.1. Thermal parameters

The analysed test pieces are basically made up of four phases: albite glass, albite crystals, quartz, and air (porosity). The effective conductivity of the mixture may be calculated using the effective medium theory (EMT) model[8-10]:

$$\sum_j V_j \frac{k_j - k_{eff}}{k_j + 2k_{eff}} = 0$$

Equation 5

where the sum extends to all components, V_j is the volume fraction of phase A_j, k_j is the thermal conductivity of A_j, and k_{eff} the effective conductivity. The volume fraction of A_j can be calculated from its mass fraction once the density of each component is known[11].

The variation of all thermal parameters with temperature was considered. The thermal conductivity of the following components was obtained from the literature: albite glass[12], albite crystal[12], quartz[13], and air[14]. Density was determined from the work of Hofmeister[12] and Ohno[15], while specific heat was determined from that of Hofmeister[12] and Hemingway[16].

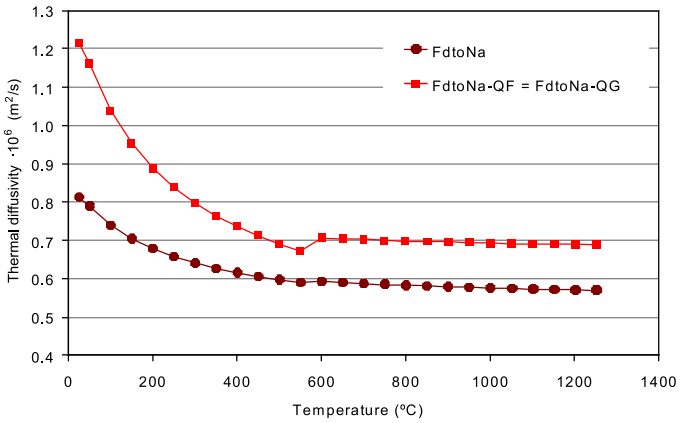

Figure 5. Thermal diffusivity of the test compositions calculated using eq. 5.

The thermal diffusivity of the test compositions, calculated with the EMT model (eq. 5), is shown in Figure 5.

4.2. MECHANICAL PARAMETERS

The two most important parameters of the mechanical simulation were the constitutive equations and the dilatometric curve.

Linear viscoelastic constitutive equations were used, in which the variation of viscosity with temperature was incorporated. This model had two parameters: the modulus of elasticity and viscosity.

4.2.1. Modulus of elasticity

The modulus of elasticity of FdtoNa, FdtoNa-QF, and FdtoNa-QG was experimentally determined using an acoustic emission apparatus (*Grindosonic*) coupled to a kiln. This apparatus enabled E to be measured up to the albite glass transformation temperature (T_g).

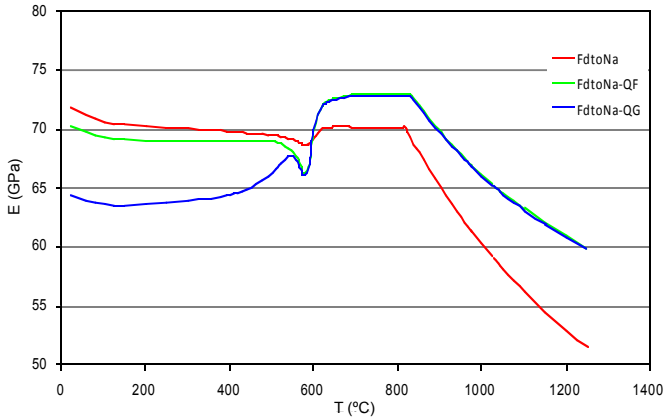

Figure 6. Evolution of the modulus of elasticity with temperature

Above this temperature, data from the literature on the modulus of elasticity of each crystalline component were used[15,17], while in the case of albite glass (E_{al}) the following expression was used[18]:

$$E_{al} = E_{al,g} \frac{T_{al,g}}{T}$$

Equation 6

where $T_{al,g}$ is the glass transition temperature (K), T the temperature (K), and $E_{al,g}$ the modulus of elasticity at the glass transition temperature (Pa). Finally, a law of mixtures (eq. 7) was used to calculate the modulus of elasticity (E_{eff}) of each test piece:

$$E_{al} = E_{al,g} \frac{T_{al,g}}{T}$$

Equation 7

where E_j is the modulus of elasticity of each phase.

4.2.2. Viscosity

Albite glass viscosity follows an equation of the Arrhenius type[4] (eq. 3). This facilitates the calculation because it suffices to know the viscosity at two temperatures. A dilatometer (*Adamel-Lhomargy, model DI-24*) was used to determine the glass transition temperature, T_g, and a hot stage microscope (*Misura HSM, model M3M 1600.80.2*) was used to quantify the half-sphere temperature, T_{s2}, these being temperatures at which it was assumed that the viscosity was 10^{12} Pa·s and $10^{3.5}$ Pa·s, respectively[19,20]. The results obtained are given in Table 2.

		Temperature (ºC)		
	η (Pa·s)	FdtoNa	FdtoNa-QF	FdtoNa-QG
T_g	10^{12}	816	830	830
T_{s2}	$10^{3.5}$	1465	1470	1470

Table 2. Glass transition temperature (T_g), half-sphere temperature (T_{s2}), and viscosity of the test compositions.

4.2.3. Dilatometric curve

The dilatometric curve was measured with a dilatometer (*Adamel-Lhomargy, model DI-24*). The curves display a shrinkage start at high temperature, owing to the load applied by the dilatometer push-rod itself and to glassy phase formation in the test pieces. This shrinkage did not occur during the cooling of the piece; in the calculation, a linear extrapolation was therefore used, shown in Figure 7.

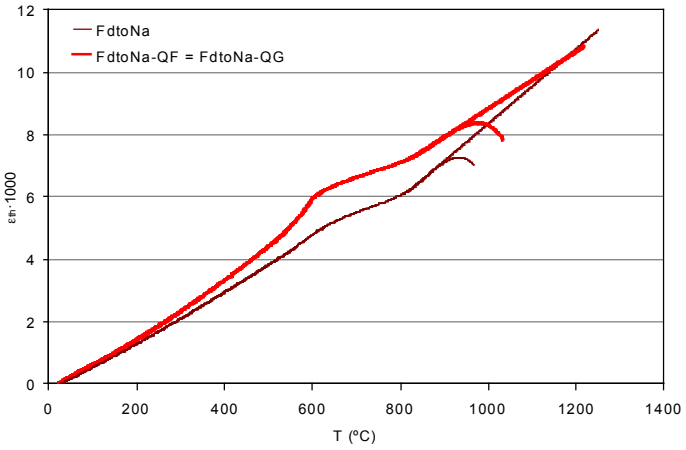

Figure 7. Dilatometric curve extrapolated with a linear section before the softening temperature

5. APPLICATION OF THE MODEL

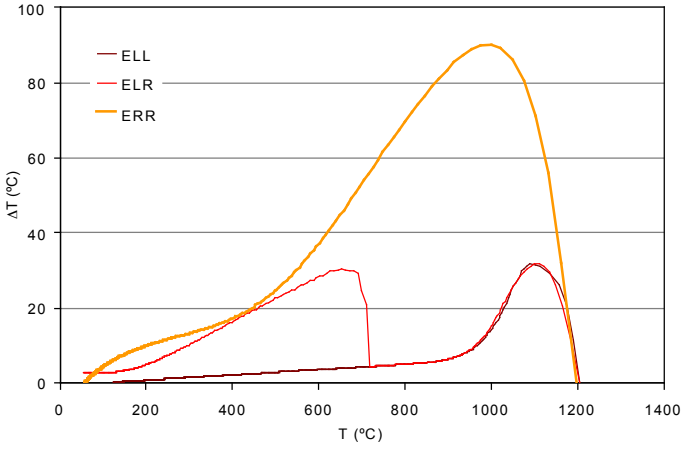

Figure 8. Thermal difference between the centre and the surface of the FdtoNa test pieces subjected to the three types of cooling

The difference in temperature between the centre and the surface of FdtoNa pieces subjected to different types of cooling is shown in Figure 8.

The evolution of the surface stresses of the FdtoNa pieces subjected to different types of cooling is shown in Figure 9.a. Stresses appeared in the centre of an opposite sign to those at the surface (not shown in order to simplify the graph). No stresses appeared above the glass transition temperature (T_g). This was due to the low viscosity of the material, which relaxed all stresses as soon as they materialised.

In the ERR cooling, stresses began to appear below T_g. A peak appeared at 573 ºC, related to the $\beta \rightarrow \alpha$ transition of the residual quartz present in the FdtoNa sample. Finally, at room temperature there was a residual stress that was not zero.

The pieces subjected to ELL cooling exhibited a low level of stress in the entire range, because the thermal gradients were of little importance. At room temperature there was a residual stress of about 1–2 MPa.

The ELR cooling was the same as the ELL cooling down to 650 ºC. Below this temperature, the pieces were extracted from the kiln and rapid cooling began, causing tensile stresses to develop that peaked at the quartz transition temperature. Once this temperature had been passed, the stresses decreased, reaching similar values to those of the ELL cooling.

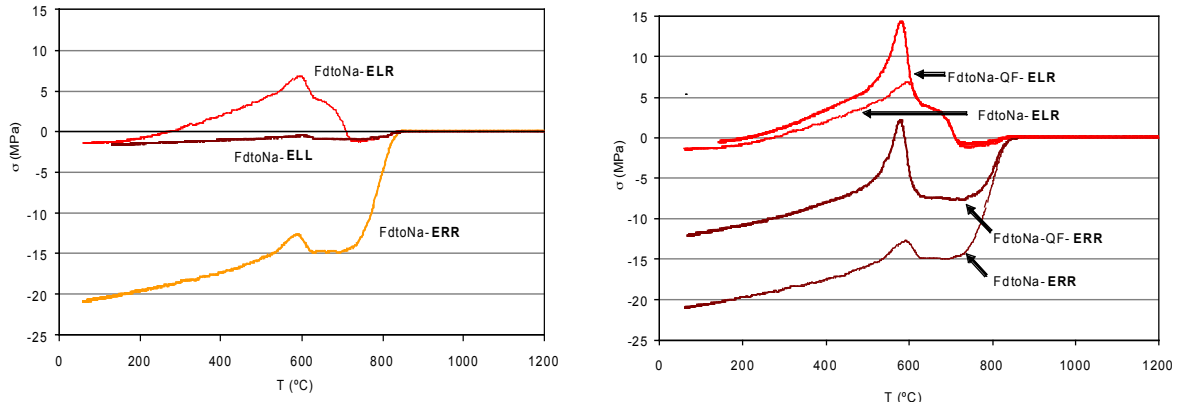

Figure 9. a) Evolution of surface stress in the FdtoNa test pieces subjected to different types of cooling. b) Effect of quartz on residual surface stress.

The graph indicates that residual stresses only appeared as a result of the thermal gradients at high temperature, slightly above T_g, as was to be expected.

The stresses were a function of the thermal history: for example, if the ELR and ERR cooling at 600 ºC (Figure 9.a) is compared, the stresses are observed to differ considerably though the difference between the temperature at the surface and in the centre was similar in both types of cooling (Figure 8). This is because

the viscous strain was very different under the two conditions as the cooling rate was quite different above T_g.

The effect of the quartz addition on the residual surface stresses for the ELR and ERR cooling may be observed in Figure 9.b. The presence of quartz induced a surface tensile stress, which explains why compositions rich in quartz tend to break more readily during industrial cooling.

On the other hand, the level of stresses produced around 700 ºC during the ERR cooling was lower when quartz was added. This was due to two factors: the composition with the quartz addition exhibited a lower coefficient of thermal expansion above 700 ºC (Figure 7) and had a greater thermal diffusivity (Figure 5). Greater thermal diffusivity meant smaller thermal differences between the surface and the centre.

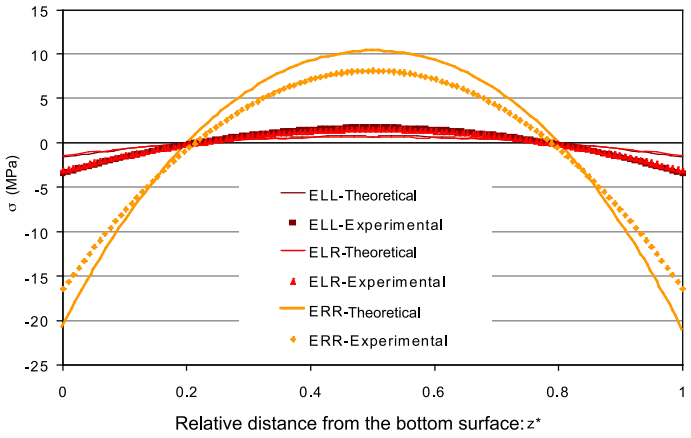

Figure 10. Experimental and theoretical residual stress profiles of the FdtoNa test pieces.

The experimental and theoretical residual stress profiles of the FdtoNa test pieces are shown in Figure 10. Those corresponding to the other test pieces were qualitatively similar. The agreement between the theoretical values and the experimental data was reasonably good, particularly if it is taken into account that the model contains no fitting parameter.

It may be observed that the stress profile was parabolic, as indicated by eq. 4, the surface being subjected to compression (negative stress) and the centre to tensile force (positive stress). This stress distribution reinforces the piece, since tile fracture usually occurs as a result of surface tensile stresses. The residual stresses were significantly higher in the ERR cooling than in the ELR and ELL cooling, in agreement with the results displayed in Figure 9.a.

The fact that the profile was parabolic means that a single parameter served to characterise it: for example, the residual surface stress can be used, as indicated in eq. 4. The theoretical and experimental results of the residual surface stresses of the different test pieces and types of cooling are compared in Figure

11. The figure shows that the results are reasonably good. In particular, the model was able to predict that the residual stresses in the ERR cooling were lower in the test pieces with the quartz addition, independently of quartz particle size.

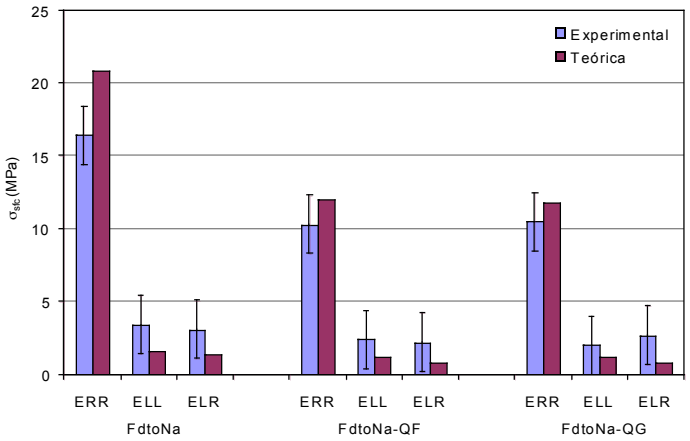

Figure 11. Residual surface stresses of the different test pieces and types of cooling analysed.

Other factors that were not analysed, such as thickness, could also influence the residual stresses. Lower thicknesses would be expected to lead to lower stresses.

6. CONCLUSIONS

- A model and a calculation methodology were developed that allow the macroscopic residual stresses produced during cooling to be estimated. The model only uses literature and laboratory test data, though it contains no fitting parameter.
- The stress profiles were parabolic. This allowed a single parameter, such as surface stress, to be used to characterise these.
- Residual stresses were only generated at high temperature. High cooling rates below T_g (for example during the allotropic transformation of quartz) led to stresses during cooling which disappeared, however, at room temperature.
- The stresses arising during cooling depended on the thermal history of the piece. In particular, the stresses in the transitional zone of quartz increased (more positive or less negative) when cooling at high temperature took place more slowly. This was because of the viscous strain that developed at high temperature.
- The allotropic $\beta \rightarrow \alpha$ transformation of quartz gave rise to a peak in the stresses during cooling.

- When quartz was added, the residual stresses were lower under the same cooling conditions. This was because, at high temperature, the quartz addition lowered the coefficient of linear expansion and increased thermal diffusivity.

ACKNOWLEDGEMENTS

The authors gratefully thank the Ministry of Science and Innovation for the funding received in the frame of the National Programme for Basic Research Projects (BIA2009-10692), and the CAPES-DGU project (Brazil: BEX 6505/10-4).

REFERENCES

[1] CANTAVELLA, V. *et al*. Evolución de las tensiones y curvaturas en soportes porosos durante el enfriamiento. In: *X World Congress on Ceramic Tile Quality - Qualicer 2008*. Castellón: Cámara oficial de comercio, industria y navegación, 2008. pp. P.BC241-P.BC255.

[2] INCROPERA, F.P.; WITT, D.P. de. *Fundamentals of heat and mass transfer*. Singapore: John Wiley & Sons, 1990.

[3] QUIROGA, A.S. *Curso de elasticidad*. Madrid: Bellisco, 1990.

[4] SCARFE, C. M.; CRONIN, D.J. Viscosity-temperature relationship of melts at 1 atm in the system diopside-albite. *American Mineralogist*, 71(5-6), 767-771, 1986.

[5] NONI, A DE JR.; HOTZA, D.; CANTAVELLA, V.; SÁNCHEZ, E. Influence of macroscopic residual stresses on the mechanical behavior and microstructure of porcelain tile. *J. Eur. Ceram. Soc.,* 28 (13), 2463-2469, 2008.

[6] LU, J. *Handbook of Measurement of Residual Stresses*. Fairmont Press, Lilburn, 1996.

[7] CANTAVELLA, V.; GARCÍA-TEN, J.; SÁNCHEZ, E.; BANNIER, E.; SÁNCHEZ, J.; SOLER, C.; SALES, J. Curvaturas diferidas en gres porcelánico. Análisis y medida de los factores que intervienen. In: *X World Congress on Ceramic Tile Quality - Qualicer 2008*. Castellón: Cámara oficial de comercio, industria y navegación, 2008. pp. P.BC207-P.BC224.

[8] DAVIS, H.T.; VALENCOURT, L.R.; JOHNSON, C.E. Transport processes in composite media. *Journal of the American Ceramic Society*, 58(9-10), 446–452, 1975.

[9] WANG, M.; PAN, N. Predictions of effective physical properties of complex multiphase materials. *Materials Science and Engineering R*, 63(1), 1–30, 2008.

[10] CARSON, J.K.; LOVATT, S.J.; TANNER, D.J. *et al*. Thermal conductivity bounds for isotropic, porous materials. *International Journal of Heat and Mass Transfer*, 48(11), 2150–2158, 2005.

[11] SCHNEIDER, S.J. Engineering properties of glass-ceramics, *Engineered Materials Handbook, Vol. 4: Ceramics and Glasses*, ASM International, USA (1991).

[12] HOFMEISTER, A.M.; WHITTINGTON, A.G.;PERTERMANN, M. Transport properties of high albite crystals, near-endmember feldspar and pyroxene glasses, and their melts to high temperature. *Contrib Mineral Petrol*, 158(3), 381–400, 2009.

[13] GIBERT, B.; MAINPRICE, D. Effect of crystal preferred orientations on the thermal diffusivity of quartz polycrystalline aggregates at high temperature. *Tectonophysics*, 465(1-4), 150–163, 2009.

[14] WEAST, R.C. Handbook of chemistry and physics. CRC Press, Cleveland, OH, 1974.

[15] OHNO, I.; HARADA, K.; YOSHITOMI, C. Temperature variation of elastic constants of quartz across the α - β transition. *Phys Chem Minerals*, 33(1), 1–9, 2006.

[16] HEMINGWAY, B.S. *Quartz: Heat Capacities from 340 to 1000K and revised values for thermodynamic properties*. *American Mineralogist*, 72, 273-279, 1987.

[17] AHRENS, I. Mineral Physics and Crystallography: A Handbook of Physical Constants. *American Geophysical Union*, 1995.

[18] ROUXEL, T. Elastic Properties and Short-to Medium-Range Order in Glasses. *J. Am. Ceram. Soc.*, 90(10), 3019–3039 (2007).

[19] MAGRINI, F.; FERRARI, R.; BRUNETTI, P. Ruolo della viscositá e della tensione superficiale nel processo di cottura delle vetrine e degli smalti ceramici.*Cerâmica Informazione*, 171, 391, 1979.

[20] NEVES, E.; POFFO, E.D.; FREDEL, M.C.; RIELLA, H.G.; ALARCON, O.E. Efeito da adição de Na_2O na viscosidade e devitrificação do vidro obtido a partir de cinzas volantes de Li_2O. *Química Nova*, 21(4), 534-537, 1998.